Electronic Supplementary Information (ESI)

Comparative study on the impact of through-space charge transfer over electroluminescence performance of delayed fluorescence molecules

Maoxing Yu, *Xiangyu Zhu*, *Jiajie Zeng*, *Hao Liu*, *Ruishan Huang*, *Zeyan Zhuang*, *Pingchuan Shen*, *Zujin Zhao*,* *and Ben Zhong Tang**

Content

S-1 General information

All the chemicals and reagents were purchased from commercial sources and used as received without further purification. The final products were subjected to vacuum sublimation to further improve purity before photoluminescence (PL) and electroluminescence (EL) properties investigations. ^{1}H and ^{13}C NMR spectra were measured on a Bruker AV 500 spectrometer in $CDCl_3$ or THF-d8 at room temperature. High resolution mass spectra (HRMS) were recorded on a GCT premier CAB 048 mass spectrometer operating in MALDI-TOF mode. Single crystals of *v*-PXZTRZ were grown in dichloromethane/ethanol mixtures and single crystal X-ray diffraction intensity data were collected on Rigaku XtaLAB P2000 FR-X with a rotating copper anode and a Pilatus 200 K detector at 150 K. UV-vis absorption spectra were measured on a Shimadzu UV-2600 spectrophotometer. PL spectra were recorded on a Horiba Fluoromax-4 spectrofluorometer. PLQY data were measured using a Hamamatsu absolute PL quantum yield spectrometer C11347 Quantaurus_QY. Transient PL decay spectra of solutions/nondoped films/doped films under room temperature and temperature-dependent transient PL decay spectra of doped films were measured using Quantaurus-Tau fluorescence lifetime measurement system (C11367-03, Hamamatsu Photonics Co., Japan). Temperature-dependent transient PL decay spectra of nondoped films were measured using Edinburgh FLS980. Cyclic voltammetry (CV) were performed on a CHI 610EA14297 in a solution of tetra-*n*-butylammonium hexafluorophosphate (Bu_4NPF_6) (0.1 M) in dichloromethane (DCM) or dimethylformamide (DMF) at a scan rate of 100 mV s^{-1}, using a platinum wire as the auxiliary electrode, a glass carbon disk as the working electrode and Ag/Ag^+ as the reference electrode. Ionization Potential (IP_{CV}) = [$E_{ox} - E_{1/2}(Fc/Fc^+) + 4.8$] eV, Electron Affinities (EA_{CV}) = [$E_{red} - E_{1/2}(Fc/Fc^+) + 4.8$] eV, where E_{ox} and E_{red} represent the onset oxidation potential and the reduction potential relative to Fc/Fc^+ (4.8 eV), respectively, and $E_{1/2}(Fc/Fc^+)$ represents the calibrated value. The ground-state geometries were optimized using the density functional theory (DFT) method with M06-2X functional at the basis set level of 6-31G*, and the ΔE_{ST} values were calculated by time-dependent DFT (TDDFT) method at the M06-2X/6-31G* level.[1] All the calculations were performed using Gaussian09 package. Differential scanning calorimetry (DSC) analysis was carried out on a DSC Q1000 under dry nitrogen at a heating rate of 10 °C min^{-1}, and thermogravimetric analysis was performed on a Netzsch TG 209 F3 under nitrogen with a heating rate of 20 °C min^{-1}.

S-2 Synthesis and characterization

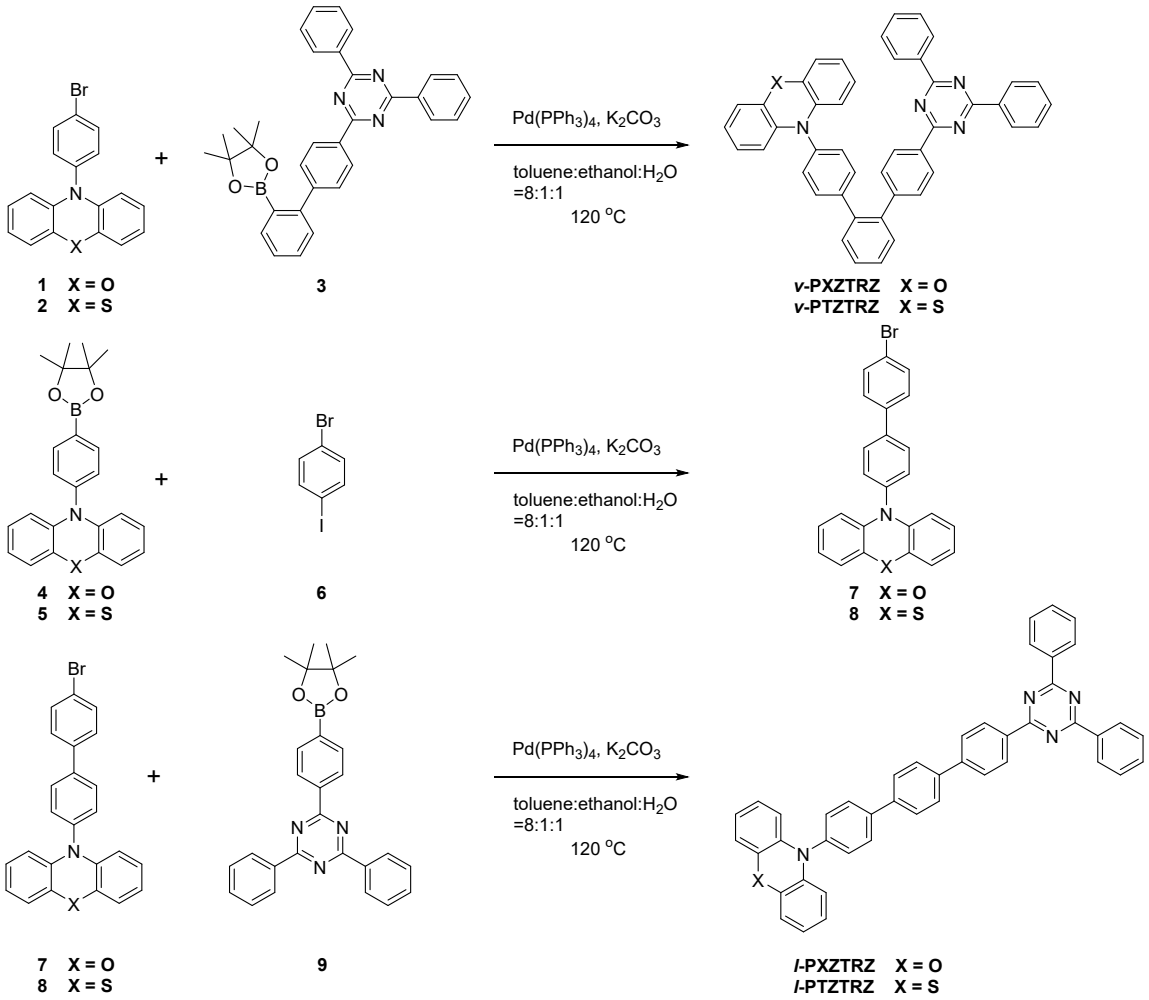

Scheme S1. Synthesis routes of *v*-PXZTRZ, *v*-PTZTRZ, *l*-PXZTRZ and *l*-PTZTRZ.

The synthetic procedures of compound 1,2, 4, 5 and 9 were referred to previous report.[2-6] The compound 3 was purchased from GeAo Chem commercial company. The compound 6 was purchased from Energy chemical company.

10-(4''-(4,6-Diphenyl-1,3,5-triazin-2-yl)-[1,1':2',1''-terphenyl]-4-yl)-10H-phenoxazine (*v*-PXZTRZ): A mixture of compound 3 2,4-diphenyl-6-(2'-(4,4,5,5-tetramethyl-1,3,2-dioxaborolan-2-yl)-[1,1'-biphenyl]-4-yl)-1,3,5-triazine (0.70 g, 1.4 mmol), compound 1 10-(4-bromophenyl)-10H-phenoxazine (0.50 g, 1.5 mmol), $Pd(PPh_3)_4$ (0.047 g, 0.041 mmol), K_2CO_3 (0.56 g, 4.1 mmol) was added in 250 mL two-neck bottle under nitrogen. Then, a mixed solvent system (50 mL) of toluene, C_2H_5OH and H_2O (v/v/v = 8:1:1) was injected into the bottle, and the reaction mixture was refluxed for 8 h. After cooling to room temperature, the mixture was poured into water and extracted twice with dichloromethane, and then dried over anhydrous magnesium sulfate. After filtration, the solvent was evaporated under reduced pressure and the residue was purified by silica gel column chromatography (petroleum ether/DCM, 3:1). Yellow solid of *v*-PXZTRZ was obtained in 74% yield. ^{1}H NMR (400

MHz, CD_3Cl, δ): 8.82–8.73 (m, 4H), 8.72–8.63 (m, 2H), 7.66–7.50 (m, 10H), 7.43–7.33 (m, 4H), 7.20 (d, J = 8.2 Hz, 2H), 6.67–6.58 (m, 4H), 6.52 (s, 2H), 5.93 (d, J = 7.5 Hz, 2H); ^{13}C NMR (100 MHz, CD_3Cl, δ): 171.77, 171.42, 145.75, 141.91, 140.38, 140.20, 136.37, 134.80, 132.80, 132.66, 130.44, 130.23, 129.10, 128.77, 128.62, 128.26, 123.41, 113.38. HRMS ($C_{45}H_{30}N_4O$): m/z 642.2422 (M^+, calcd 642.2420).

10-(4''-(4,6-Diphenyl-1,3,5-triazin-2-yl)-[1,1':2',1''-terphenyl]-4-yl)-10H-phenothiazine (*v*-PTZTRZ): A mixture of compound 3 (0.70 g, 1.4 mmol), compound 2 10-(4-bromophenyl)-10H-phenothiazine (0.53 g, 1.5 mmol), $Pd(PPh_3)_4$ (0.047 g, 0.041 mmol), K_2CO_3 (0.56 g, 4.1 mmol) was added in 250 mL two-neck bottle under nitrogen. Then, a mixed solvent system (50 mL) of toluene, C_2H_5OH and H_2O (v/v/v = 8:1:1) was injected into the bottle, and the reaction mixture was refluxed for 8 h. After cooling to room temperature, the mixture was poured into water and extracted twice with dichloromethane, and then dried over anhydrous magnesium sulfate. After filtration, the solvent was evaporated under reduced pressure and the residue was purified by silica gel column chromatography (petroleum ether/DCM, 3:1). Yellow solid of *v*-PTZTRZ was obtained in 70% yield. ^{1}H NMR (400 MHz, CD_3Cl, δ): 8.80–8.75 (m, 4H), 8.72–8.67 (m, 2H), 7.65–7.51 (m, 10H), 7.46–7.32 (m, 4H), 7.25 (s, 2H), 7.06–6.37 (m, 6H), 6.18 (s, 2H); ^{13}C NMR (125 MHz, CD_3Cl, δ): 171.58, 171.20, 145.63, 141.46, 140.20, 140.13, 136.15, 134.55, 132.53, 132.37, 130.33, 130.22, 130.03, 128.93, 128.63, 128.43, 128.10, 126.88, 115.99. HRMS ($C_{45}H_{30}N_4S$): m/z 658.2194 (M^+, calcd 658.2191).

10-(4'-Bromo-[1,1'-biphenyl]-4-yl)-10H-phenoxazine (7): A mixture of compound 4 10-(4-(4,4,5,5-tetramethyl-1,3,2-dioxaborolan-2-yl)phlenyl)-10H-phenoxazine (1.44 g, 3.8 mmol), compound 6 1-bromo-4-iodobenzene (1.27 g, 4.5 mmol), $Pd(PPh_3)_4$ (0.13 g, 0.11mmol), K_2CO_3 (1.55 g, 11 mmol) was added in 250 mL two-neck bottle under nitrogen. Then, a mixed solvent system (60 mL) of toluene, C_2H_5OH and H_2O (v/v/v = 8:1:1) was injected into the bottle, and the reaction mixture was refluxed for 8 h. After cooling to room temperature, the mixture was poured into water and extracted twice with dichloromethane, and then dried over anhydrous magnesium sulfate. After filtration, the solvent was evaporated under reduced pressure and the residue was purified by silica gel column chromatography (petroleum ether/DCM, 10:1). White solid of 7 was obtained in 68% yield. ^{1}H NMR (500 MHz, CD_3Cl, δ): 7.77 (d, J = 8.0 Hz, 2H), 7.62 (d, J = 8.1 Hz, 2H), 7.52 (d, J = 8.2 Hz, 2H), 7.41 (d, J = 7.6 Hz, 2H), 6.73–6.56 (m, 6H), 5.99 (d, J = 7.8 Hz, 2H); ^{13}C NMR (125 MHz, CD_3Cl, δ): 144.05, 140.25, 139.12, 138.52, 134.38, 132.20, 131.44, 129.65, 128.88, 123.38, 122.24, 121.53, 115.60, 113.37. HRMS ($C_{24}H_{16}BrNO$): m/z 413.0399 (M^+, calcd 413.0415).

10-(4'-Bromo-[1,1'-biphenyl]-4-yl)-10H-phenothiazine (8): A mixture of compound 5,10-(4-

(4,4,5,5-tetramethyl-1,3,2-dioxaborolan-2-yl)phenyl)-10H-phenothiazine (1.50 g, 3.8 mmol), compound 6 (1.27 g, 4.5 mmol), $Pd(PPh_3)_4$ (0.13 g, 0.11mmol), K_2CO_3 (1.55 g, 11 mmol) was added in 250 mL two-neck bottle under nitrogen. Then, a mixed solvent system (60 mL) of toluene, C_2H_5OH and H_2O (v/v/v = 8:1:1) was injected into the bottle, and the reaction mixture was refluxed for 8 h. After cooling to room temperature, the mixture was poured into water and extracted twice with dichloromethane, and then dried over anhydrous magnesium sulfate. After filtration, the solvent was evaporated under reduced pressure and the residue was purified by silica gel column chromatography (petroleum ether/DCM, 10:1). White solid of 8 was obtained in 81% yield. ^{1}H NMR (500 MHz, CD_3Cl, δ): 7.76 (d, J = 7.4 Hz, 2H), 7.62–7.59 (m, 2H), 7.53–7.51 (m, 2H), 7.44 (d, J = 8.0 Hz, 2H), 7.06–7.04 (m, 2H), 6.88 (s, 4H), 6.32 (s, 2H). ^{13}C NMR (125 MHz, CD_3Cl, δ): 139.49, 139.01, 132.03, 129.12, 128.70, 126.87, 121.99, 116.48. HRMS ($C_{24}H_{16}BrNS$): m/z 429.0187 (M^+, calcd 429.0151).

10-(4''-(4,6-Diphenyl-1,3,5-triazin-2-yl)-[1,1':4',1''-terphenyl]-4-yl)-10H-phenoxazine (*l*-PXZTRZ): A mixture of compound 7 (0.62 g, 1.5 mmol), compound 9 2,4-diphenyl-6-(4-(4,4,5,5-tetramethyl-1,3,2-dioxaborolan-2-yl)phenyl)-1,3,5-triazine (0.78 g, 1.8 mmol), $Pd(PPh_3)_4$ (0.052 g, 0.045 mmol), K_2CO_3 (0.62 g, 4.5 mmol) was added in 250 mL two-neck bottle under nitrogen. Then, a mixed solvent system (50 mL) of toluene, C_2H_5OH and H_2O (v/v/v = 8:1:1) was injected into the bottle, and the reaction mixture was refluxed for 8 h. After cooling to room temperature, the mixture was poured into water and extracted twice with dichloromethane, and then dried over anhydrous magnesium sulfate. After filtration, the solvent was evaporated under reduced pressure and the residue was purified by silica gel column chromatography (petroleum ether/DCM, 3:1). Yellow solid of *l*-PXZTRZ was obtained in 46% yield. ^{1}H NMR (400 MHz, THF-d8, δ): 8.95–8.90 (m, 2H), 8.88–8.81 (m, 4H), 8.06–7.86 (m, 8H), 7.67–7.57 (m, 6H), 7.53–7.46 (m, 2H), 6.70–6.54 (m, 6H), 6.04–5.99 (m, 2H). HRMS ($C_{45}H_{30}N_4O$): m/z 642.2425 (M^+, calcd 642.2420).

10-(4''-(4,6-Diphenyl-1,3,5-triazin-2-yl)-[1,1':4',1''-terphenyl]-4-yl)-10H-phenothiazine (*l*-PTZTRZ) : A mixture of compound 8 (0.61 g, 1.4 mmol), compound 9 2,4-diphenyl-6-(4-(4,4,5,5-tetramethyl-1,3,2-dioxaborolan-2-yl)phenyl)-1,3,5-triazine (0.74 g, 1.7 mmol), $Pd(PPh_3)_4$ (0.049 g, 0.043 mmol), K_2CO_3 (0.59 g, 4.3 mmol) was added in 250 mL two-neck bottle under nitrogen. Then, a mixed solvent system (50 mL) of toluene, C_2H_5OH and H_2O (v/v/v = 8:1:1) was injected into the bottle, and the reaction mixture was refluxed for 8 h. After cooling to room temperature, the mixture was poured into water and extracted twice with dichloromethane, and then dried over anhydrous magnesium sulfate. After filtration, the solvent was evaporated under reduced pressure and the residue was purified by silica gel column chromatography (petroleum ether/DCM, 3:1). Yellow solid of *l*-PTZTRZ was obtained in 54% yield. ^{1}H NMR (400 MHz, THF-d8, δ): 8.96–8.90 (m, 2H), 8.87–8.81 (m, 4H), 8.04–

7.87 (m, 8H), 7.67–7.56 (m, 6H), 7.55–7.48 (m, 2H), 7.02 (dd, J = 7.4, 1.6 Hz, 2H), 6.91–6.78 (m, 4H), 6.36 (dd, J = 8.2, 1.2 Hz, 2H). HRMS ($C_{45}H_{30}N_4S$): m/z 658.2198 (M^+, calcd 658.2191).

S-3 Thermal stability and electrochemical property

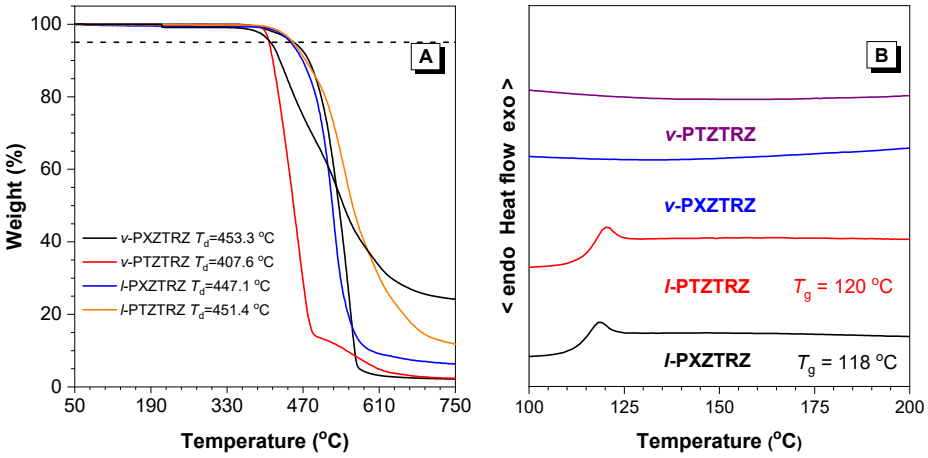

Fig. S1 (A) TGA curves and (B) differential scanning calorimetry curves of *v*-PXZTRZ, *v*-PTZTRZ, *l*-PXZTRZ and *l*-PTZTRZ, recorded under nitrogen at a heating rate of 20 °C min^{-1}.

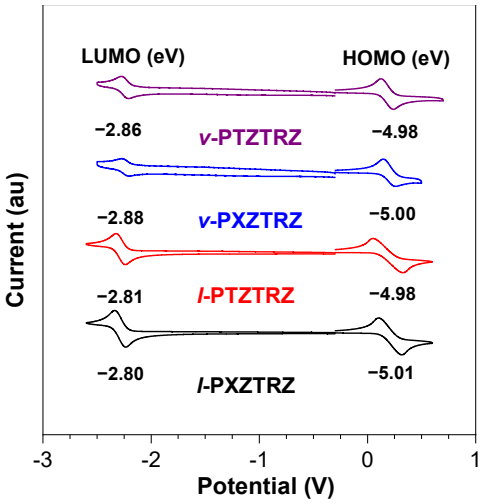

Fig. S2 Cyclic voltammograms of *v*-PXZTRZ, *v*-PTZTRZ, *l*-PXZTRZ and *l*-PTZTRZ, measured in DCM/DMF containing 0.1 m tetra-*n*-butylammonium hexafluorophosphate.

S-4 X-ray crystallography

***v*-PXZTRZ (CCDC 2055132)**: $C_{45}H_{30}N_4O$, M_W = 642.73, triclinic, P -1, a = 10.27944(16) Å, b = 14.58551(17) Å, c = 21.6209(2) Å, α = 92.8736(9)°, β = 98.7840(12)°, γ = 90.0587(11)°, V = 3199.47(7) Å^3, Z = 4, D_c = 1.334 g cm^{-3}, μ = 0.633 mm^{-1} (CuKα, λ = 1.54184), F(000) = 1344, T = 149.99(10) K, $2\theta_{max}$ = 67.684° (98.3%), 32285 measured reflections, 12344 independent reflections (R_{int} = 0.0295),

GOF on F^2 = 1.011, R_1 = 0.0492, wR_2 = 0.1198 (all data), Δe 0.195 and –0.168 eÅ^{-3}.

S-5 Photophysical properties and theoretical calculation

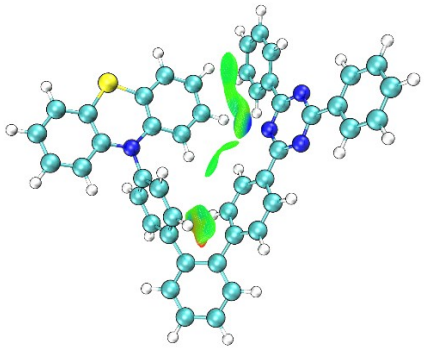

Fig. S3 Visualization of through-space conjugation of *v*-PTZTRZ, calculated based on the basis of the optimized excited-state conformation.

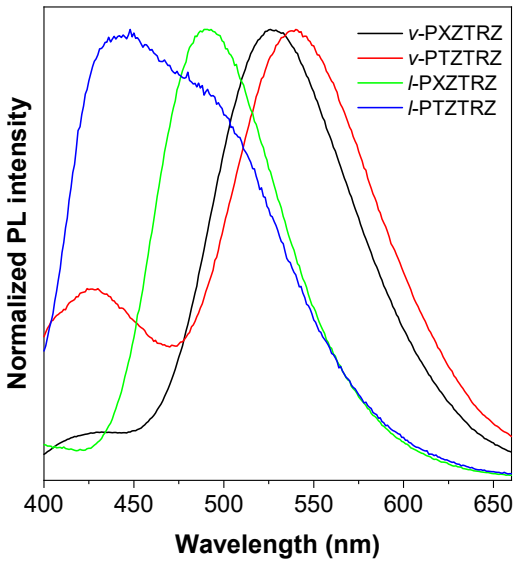

Fig. S4 Normalized PL spectra of *v*-PXZTRZ, *v*-PTZTRZ, *l*-PXZTRZ and *l*-PTZTRZ in toluene at room temperature.

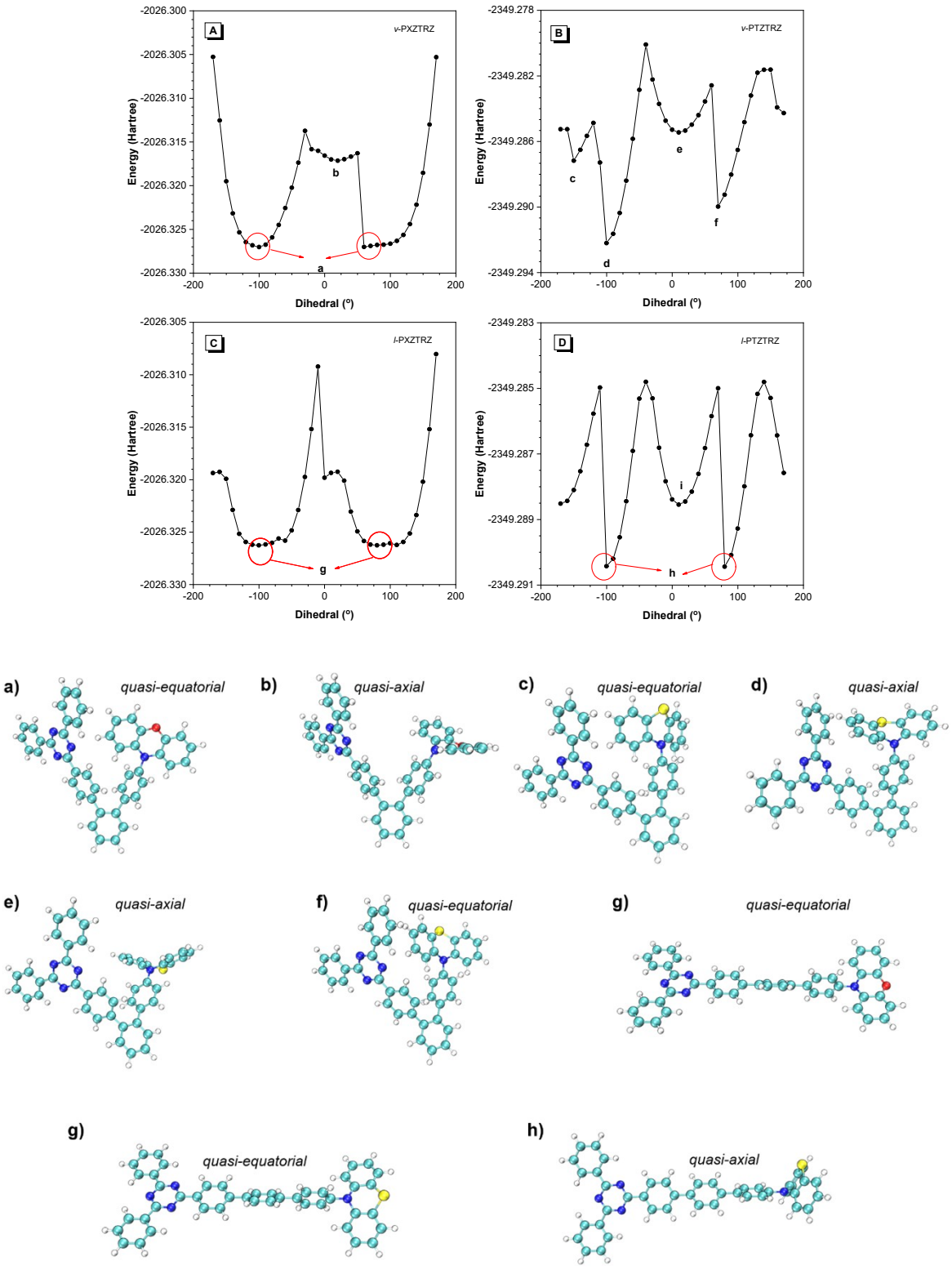

Fig. S5 Potential energy surface of the ground states under vacuum for (A) *v*-PXZTRZ, (B) *v*-PTZTRZ, (C) *l*-PXZTRZ, (D) *l*-PTZTRZ at the M06-2X/6-31G* level, respectively, and the corresponding stable and metastable conformations.

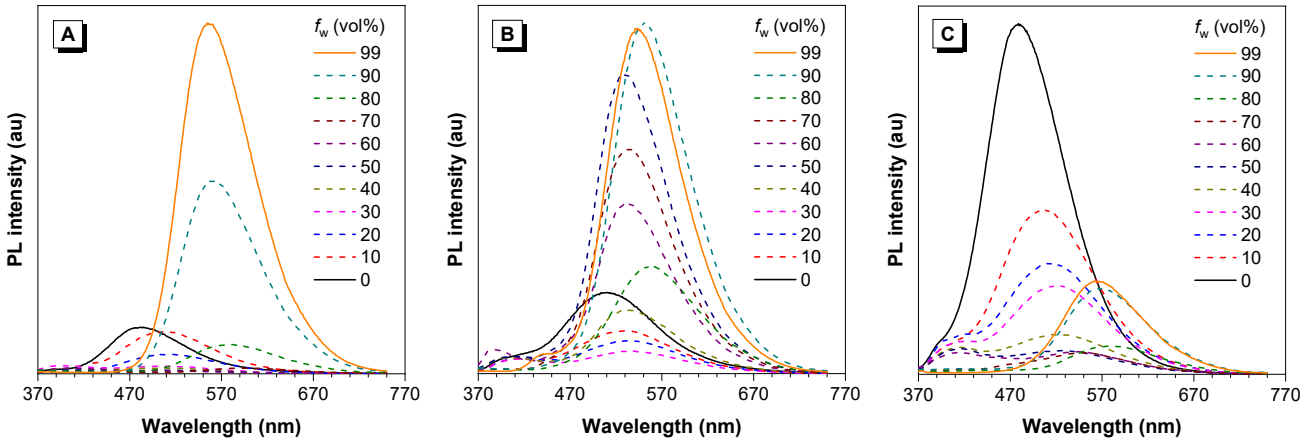

Fig. S6 PL spectra of (A) *v*-PTZTRZ, (B) *l*-PXZTRZ, (C) *l*-PTZTRZ in THF/water mixtures with different water fractions (f_w).

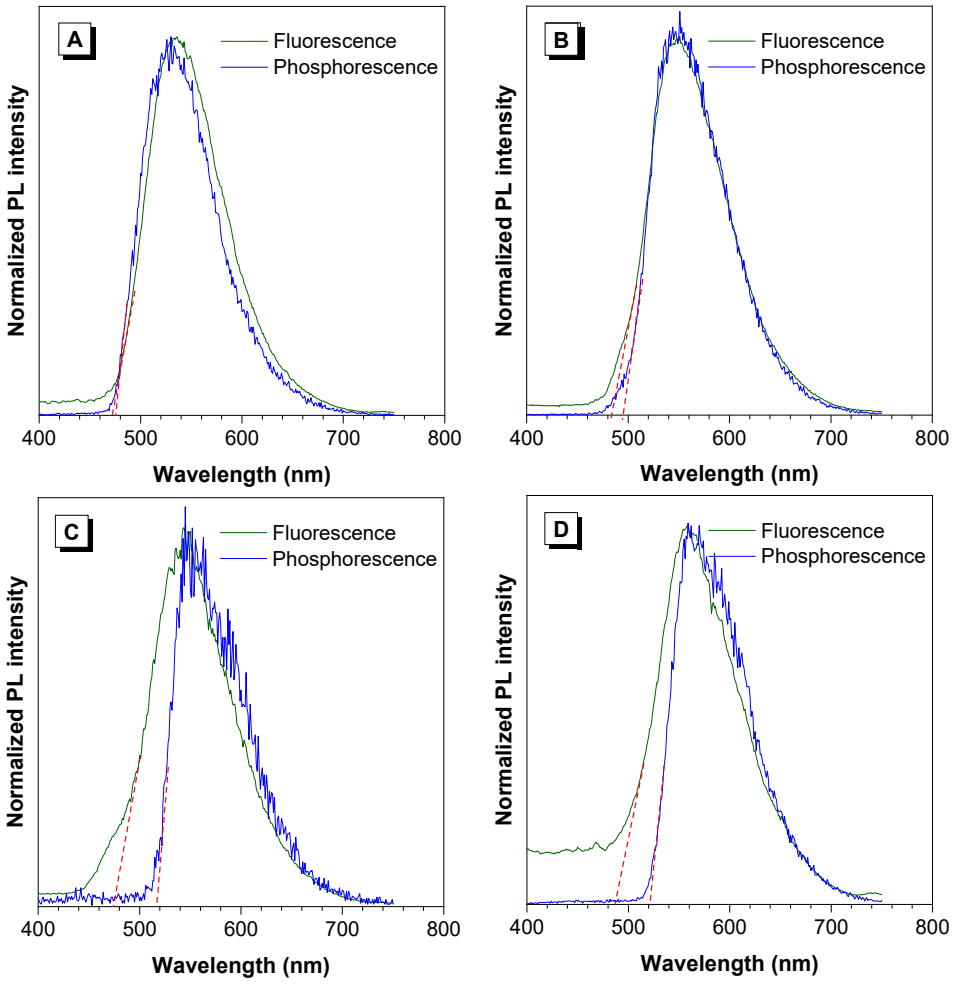

Fig. S7 Fluorescence and phosphorescence spectra of the neat films of (A) *v*-PXZTRZ, (B) *v*-PTZTRZ, (C) *l*-PXZTRZ and (D) *l*-PTZTRZ measured at 77 K under nitrogen.

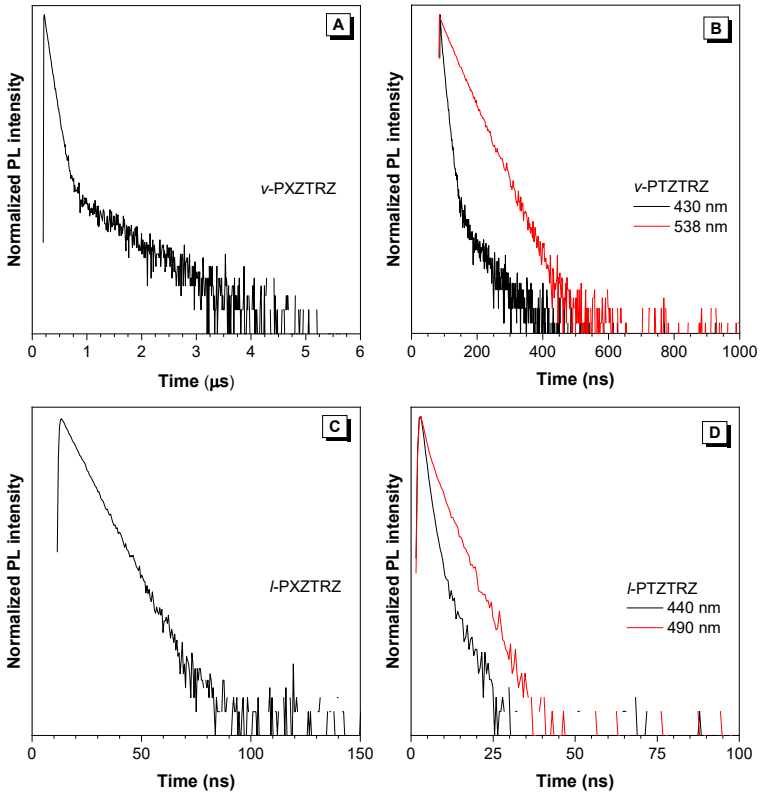

Fig. S8 Transient PL decay spectra of (A) *v*-PTZTRZ, (B) *l*-PXZTRZ, (C) *l*-PTZTRZ in toluene solutions.

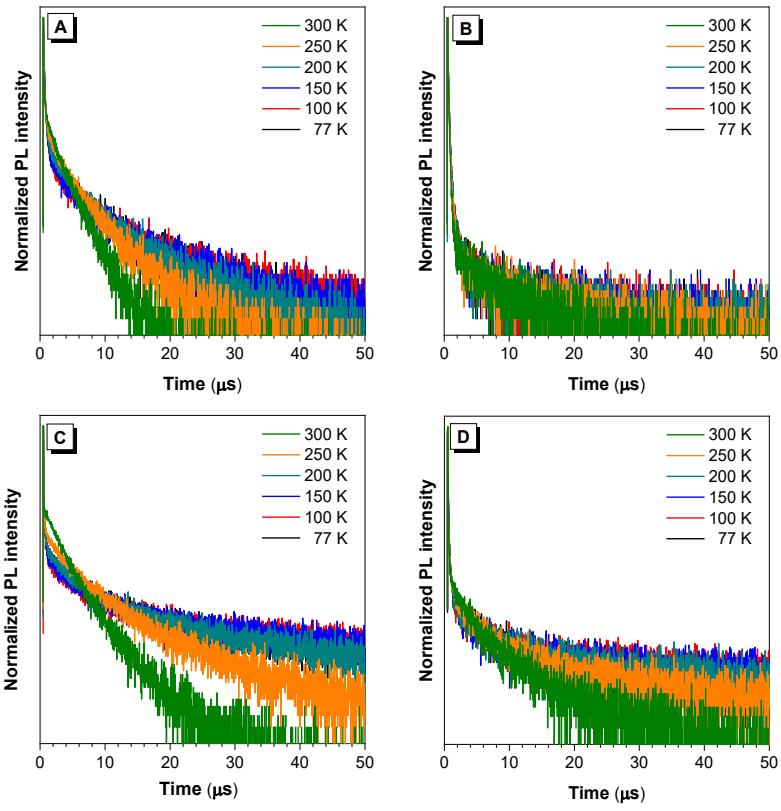

Fig. S9 Temperature-dependent transient PL decay spectra of the neat films of (A) *v*-PXZTRZ, (B) *v*-

PTZTRZ, (C) *l*-PXZTRZ and (D) *l*-PTZTRZ measured under nitrogen.

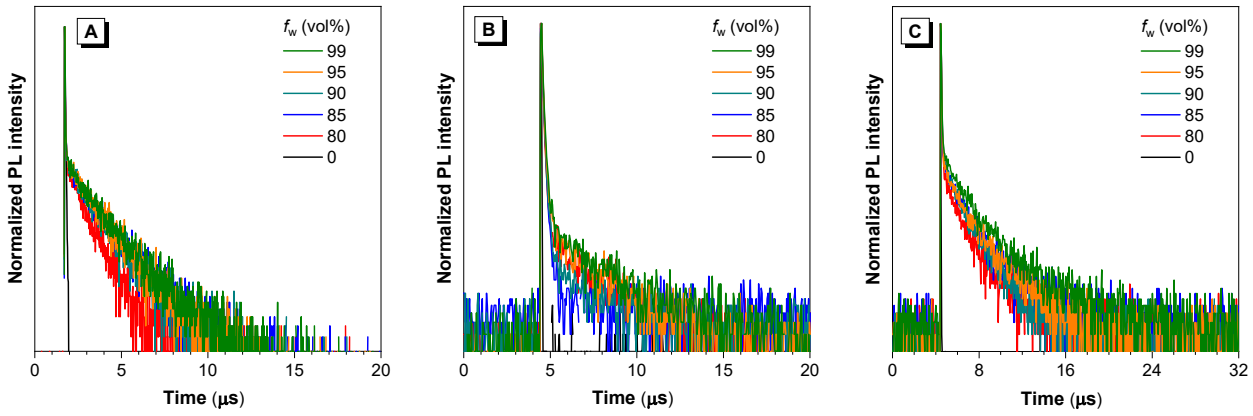

Fig. S10 Transient PL decay spectra of (A) *v*-PTZTRZ, (B) *l*-PXZTRZ, (C) *l*-PTZTRZ in THF/water mixtures with different water fractions (f_w).

S-6 Device fabrication

Glass substrates precoated with a 90 nm layer of indium tin oxide (ITO) with a sheet resistance of 15 ~ 20 Ω per square were successively cleaned in ultrasonic bath of acetone, isopropanol, detergent, and deionized water, respectively, taking 10 minutes for each procedure. Then, the substrates were totally dried in a 70 ℃ oven. Before the fabrication processes, the substrates were treated by O^2 plasma for 10 minutes to improve the hole injection ability of ITO. The vacuum-deposited OLEDs were fabricated under a pressure of $< 5 \times 10^{-4}$ Pa in the Fangsheng OMV-FS380 vacuum deposition system. Deposition rate of organic materials, LiF and Al are 1~2 A s^{-1}, 0.1 A $s^{-1}$and 5 A s^{-1}, respectively. For monochromatic OLEDs, the luminance–voltage–current density characteristics and electroluminescent spectra were obtained via a Konica Minolta CS-200 Color and Luminance Meter and an Ocean Optics USB 2000+ spectrometer, along with a Keithley 2400 Source Meter. The external quantum efficiencies were estimated utilizing the normalized EL spectra and the current efficiencies of the devices, assuming that the devices are Lambertian emitters. The effective emitting area of the devices was 9 mm^2, determined by the overlap between anode and cathode. All the characterizations were conducted at room temperature in ambient conditions without any encapsulation, as soon as the devices were fabricated.

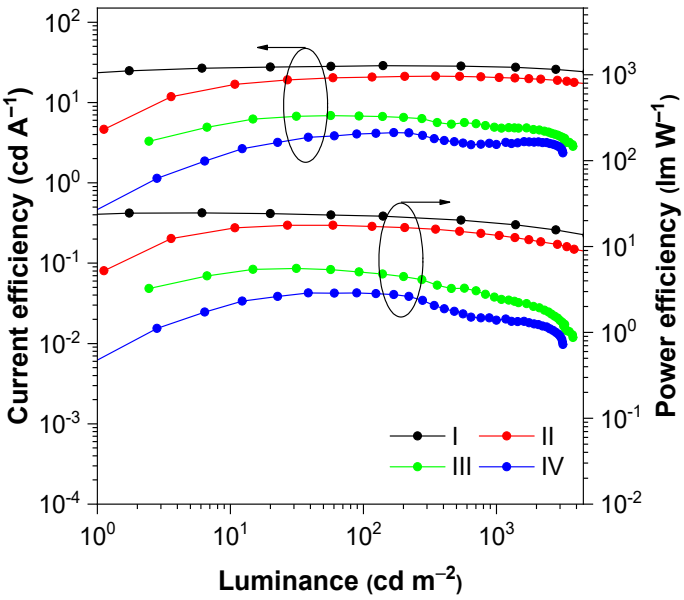

Fig. S11 Plots of (A) current efficiency−luminance−power efficiency of the nondoped OLEDs I, II, III and IV based on *v*-PXZTRZ, *v*-PTZTRZ, *l*-PXZTRZ and *l*-PTZTRZ, respectively. Device configuration: ITO/HATCN (5 nm)/TAPC (20 nm)/TcTa (5 nm)/emitter (35 nm)/TmPyPB (55 nm)/LiF (1 nm)/Al.

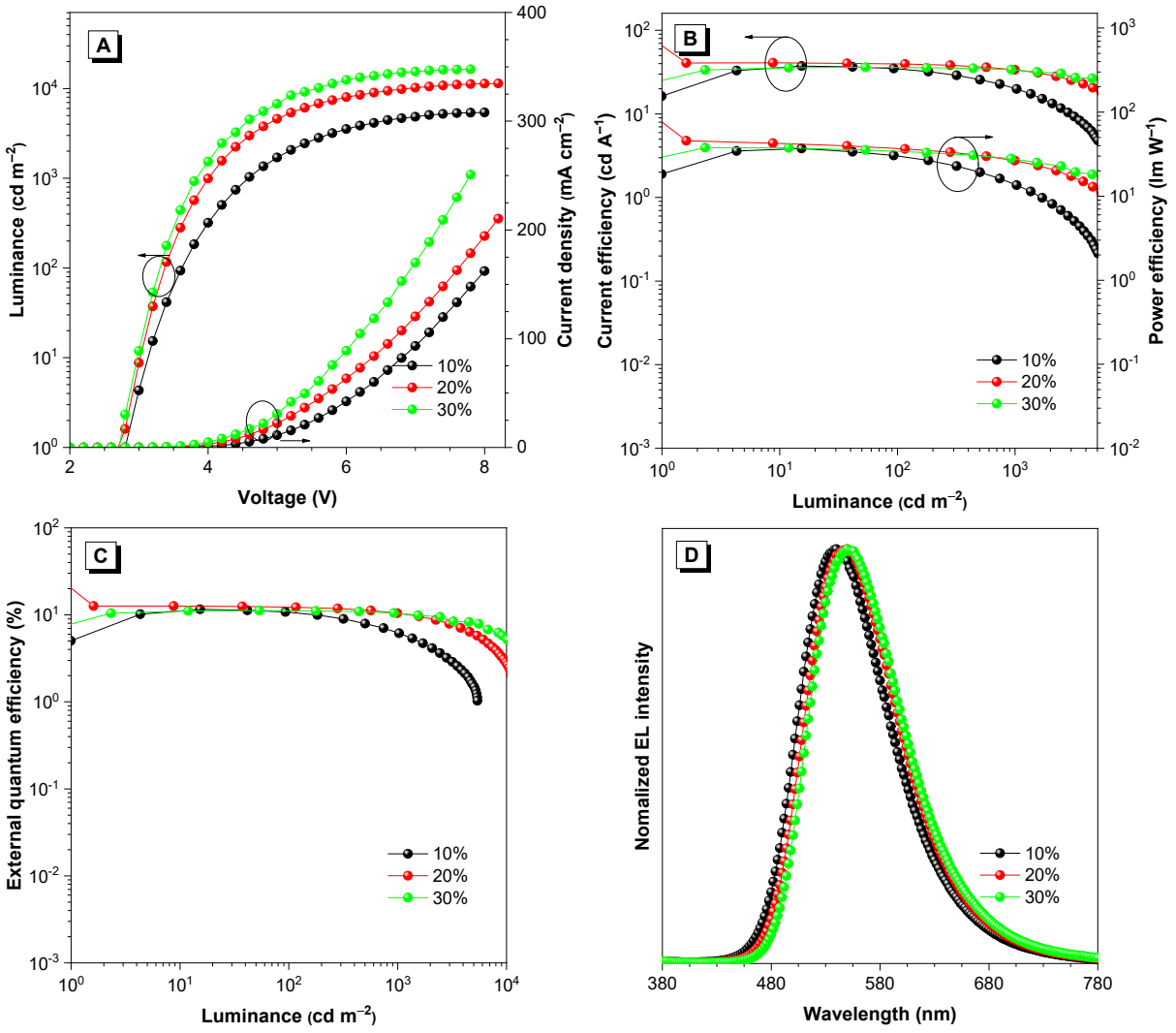

Fig. S12 Plots of (A) luminance−voltage−current density, (B) current efficiency−luminance−power efficiency, (C) external quantum efficiency−luminance and (D) EL spectra at 1000 cd m^{-2} of the doped OLEDs. Device configuration: ITO/HATCN (5 nm)/TAPC (50 nm)/TCTA (5 nm)/x wt% *v*-PXZTRZ: TmPyPB (20 nm)/TmPyPB (40 nm)/LiF (1 nm)/Al (*x* = 10, 20, 30).

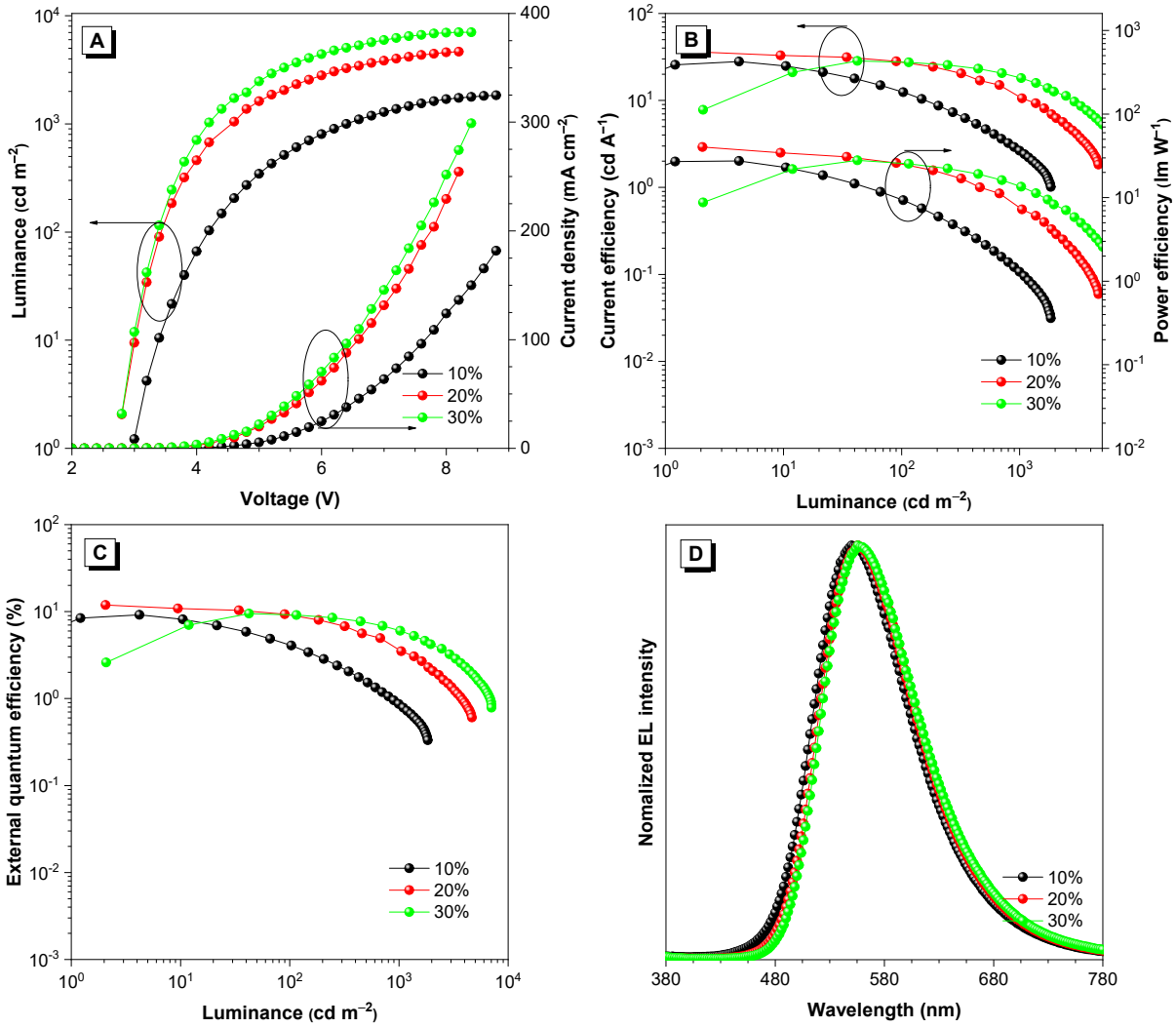

Fig. S13 Plots of (A) luminance−voltage−current density, (B) current efficiency−luminance−power efficiency, (C) external quantum efficiency−luminance of the doped OLEDs and (D) EL spectra at 1000 cd m^{-2}. Device configuration: ITO/HATCN (5 nm)/TAPC (50 nm)/TCTA (5 nm)/x wt% *v*-PTZTRZ: TmPyPB (20 nm)/TmPyPB (40 nm)/LiF (1 nm)/Al (*x* = 10, 20, 30).

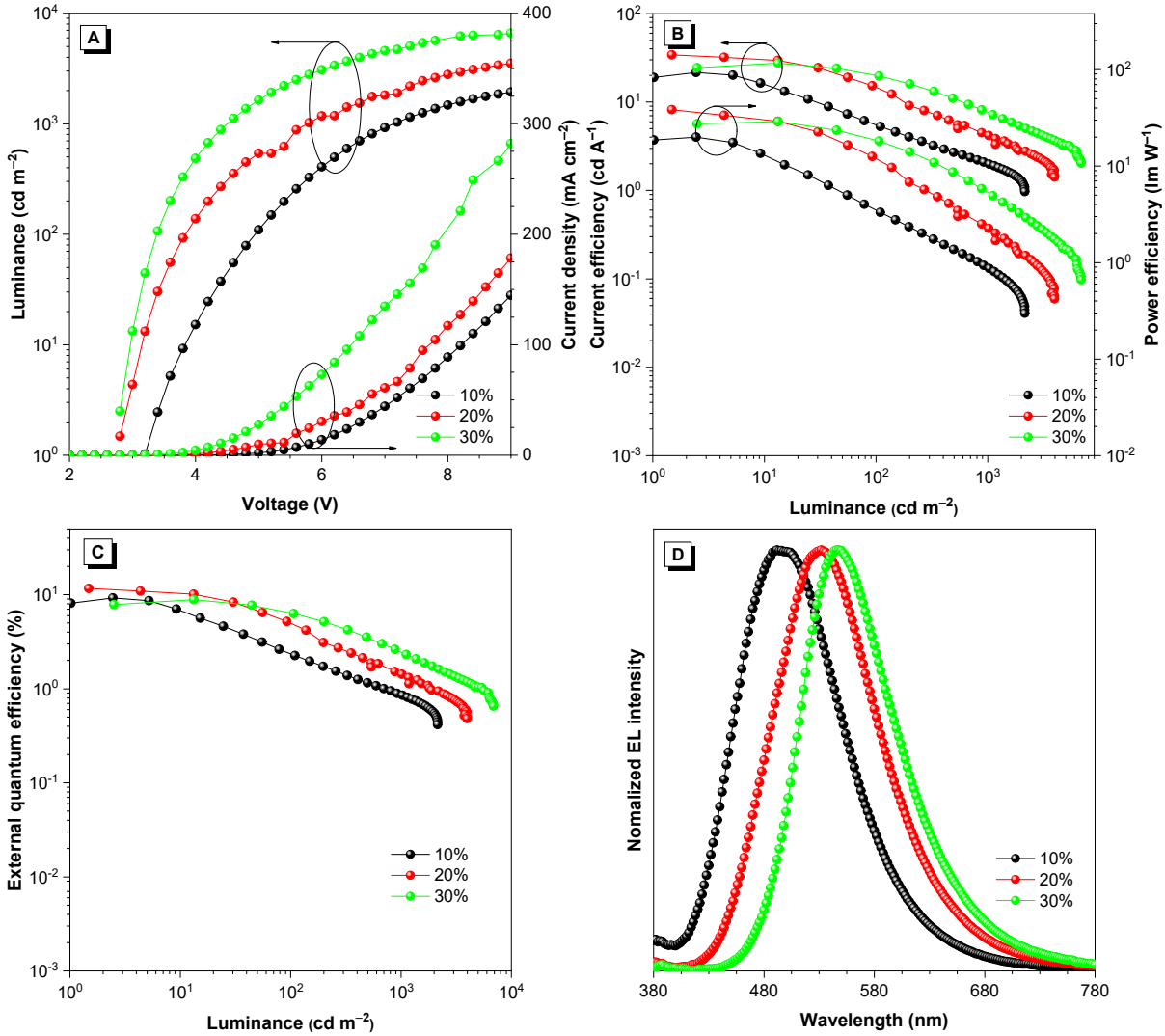

Fig. S14 Plots of (A) luminance−voltage−current density, (B) current efficiency−luminance−power efficiency, (C) external quantum efficiency−luminance and (D) EL spectra at 1000 cd m^{-2} of the doped OLEDs. Device configuration: ITO/HATCN (5 nm)/TAPC (50 nm)/TCTA (5 nm)/*x* wt% *l*-PXZTRZ: TmPyPB (20 nm)/TmPyPB (40 nm)/LiF (1 nm)/Al (*x* = 10, 20, 30).

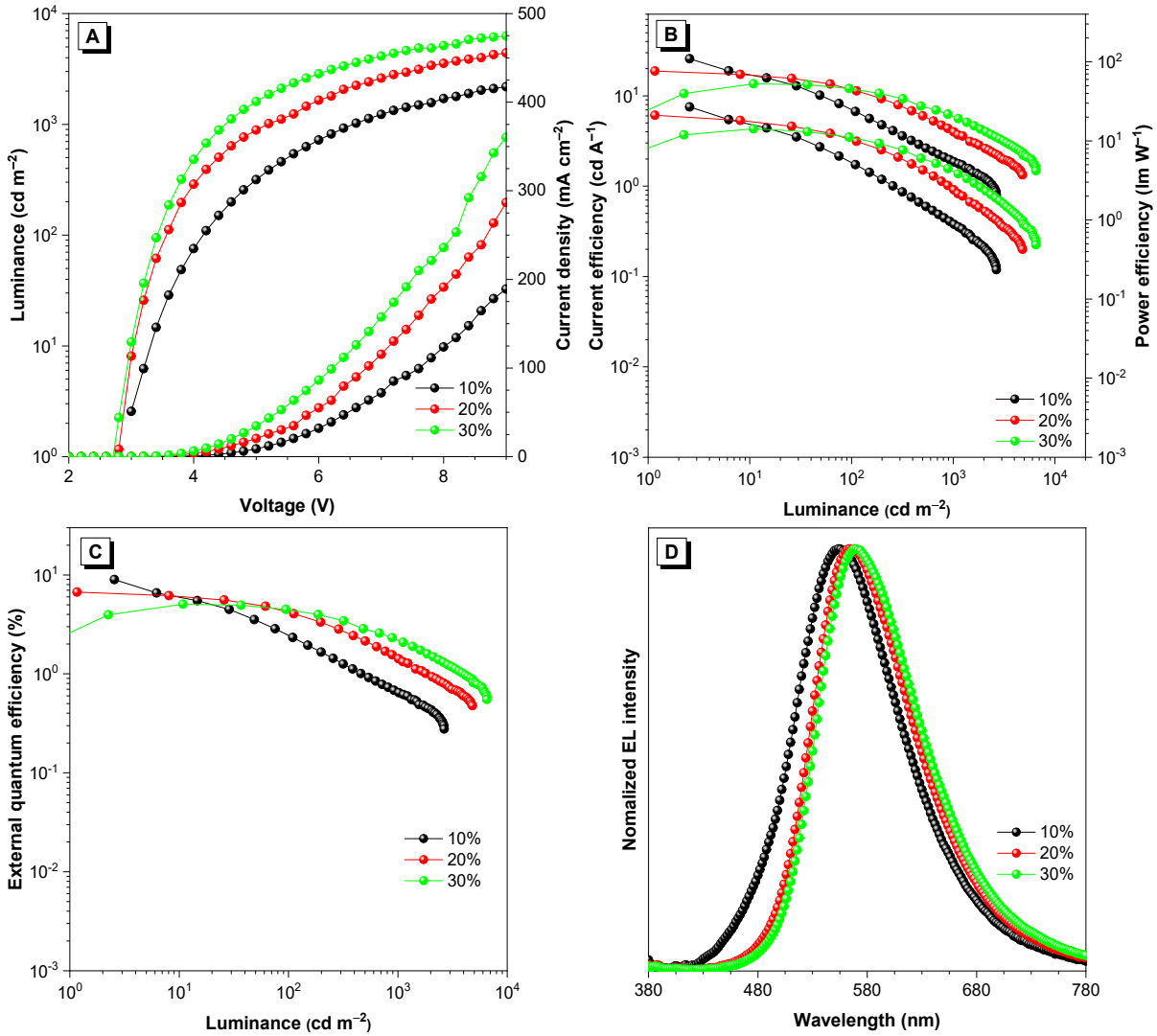

Fig. S15 Plots of (A) luminance−voltage−current density, (B) current efficiency−luminance−power efficiency, (C) external quantum efficiency−luminance and (D) EL spectra at 1000 cd m^{-2} of the doped OLEDs. Device configuration: ITO/HATCN (5 nm)/TAPC (50 nm)/TCTA (5 nm)/x wt% *l*-PTZTRZ: TmPyPB (20 nm)/TmPyPB (40 nm)/LiF (1 nm)/Al (x = 10, 20, 30).

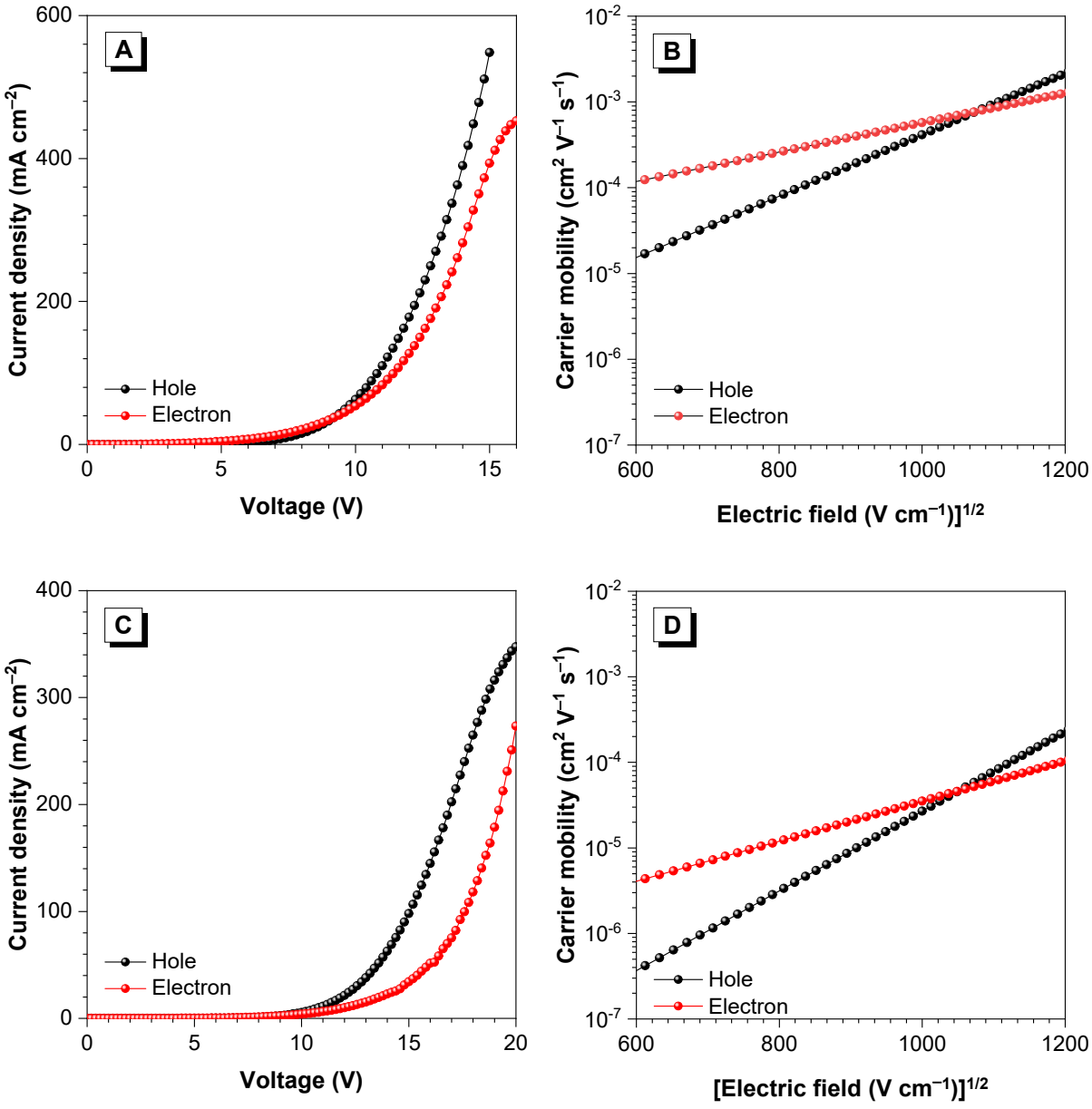

Fig. S16 Plots of (A) current density–voltage of devices H1 (hole) and E1 (electron). (B) Electric field-dependent mobilities (μ) of *v*-PXZTRZ. (C) Plots of current density–voltage of devices H2 (hole) and E2 (electron). (D) Electric field-dependent mobilities (μ) of 20% *v*-PXZTRZ: TmPyPB. Device configuration: ITO/TAPC (10 nm)/emitter (80 nm)/TAPC (10 nm)/Al, emitter = *v*-PXZTRZ and 20% *v*-PXZTRZ: TmPyPB for hole-only devices H1 and H2; ITO/TmPyPB (10 nm)/emitter (80 nm)/TmPyPB (10 nm)/LiF (1 nm)/Al, emitter = *v*-PXZTRZ and 20% *v*-PXZTRZ: TmPyPB for electron-only devices E1 and E2.

S-7 Additional spectra and data

Table S1. Photophysical data of *v*-PXZTRZ, *v*-PTZTRZ, *l*-PXZTRZ and *l*-PTZTRZ in neat films and 20 wt% *v*-PXZTRZ and 20 wt% *v*-PTZTRZ in doped films at doping concentrations of 20 wt%.[a]

	v-PXZTRZ	*v*-PTZTRZ	*l*-PXZTRZ	*l*-PTZTRZ	20 wt% *v*-PXZTRZ	20 wt% *v*-PTZTRZ
Φ_{PL} (%)	28.7	27.2	15.7	12.4	44.3	31.7
τ_{prompt} (ns)	49.1	24.1	77.9	34.8	109.2	61.3
$\tau_{delayed}$ (μs)	1.6	2.8	2	2.2	2.9	14.7
R_{prompt} (%)	27.4	18.3	87.4	56.4	25.5	20.2
$R_{delayed}$ (%)	72.6	81.7	12.6	43.6	74.5	79.8
Φ_{prompt} (%)	7.9	5.0	13.7	7.0	11.3	6.4
$\Phi_{delayed}$ (%)	20.8	22.2	2.0	5.4	33.0	25.3
Φ_{IC} (%)	19.5	13.3	73.7	49.4	14.2	13.8
Φ_{ISC} (%)	72.6	81.7	12.6	43.6	74.5	79.8
Φ_{RISC} (%)	28.7	27.2	15.7	12.4	44.3	31.7
K_F ($\times 10^6$ s^{-1})	1.6	2.1	1.8	2.0	1.0	1.0
K_{IC} ($\times 10^6$ s^{-1})	4.0	5.5	9.5	14.2	1.3	2.3
K_{ISC} ($\times 10^7$ s^{-1})	1.5	3.4	0.2	1.2	6.8	1.3
K_{RISC} ($\times 10^6$ s^{-1})	2.3	2.0	0.6	0.8	1.4	0.3

[a] Abbreviations: Φ_{PL} = absolute photoluminescence quantum yield; τ_{prompt} and $\tau_{delayed}$ = lifetimes calculated from the prompt and delayed fluorescence decay, respectively; $R_{delayed}$ = the ratio of delayed components; Φ_{prompt} and $\Phi_{delayed}$ = prompt and delayed components, respectively, determined from the total Φ_{PL} and the proportion of the integrated area of each component in the transient spectra to the total integrated area; Φ_{ISC} = the intersystem crossing quantum yield; k_F = fluorescence decay rate; k_{IC} = internal conversion decay rate from S_1 to S_0; k_{ISC} = intersystem crossing decay rate from S_1 to T_1; k_{RISC} = the rate constant of reverse intersystem crossing process. The quantum efficiencies and rate constants were determined using the following equations according to Adachi's method.[7-9]

$$\Phi_{prompt} = \Phi_{PL} R_{prompt}$$

$$\Phi_{delayed} = \Phi_{PL} R_{delayed}$$

$$k_F = \Phi_{prompt} / \tau_{prompt}$$

$$\Phi_{PL} = k_F / (k_F + k_{IC})$$

$$\Phi_{prompt} = k_F / (k_F + k_{IC} + k_{ISC})$$

$$\Phi_{IC} = k_{IC} / (k_F + k_{IC} + k_{ISC})$$

$\Phi_{ISC} = k_{ISC}/(k_F + k_{IC} + k_{ISC}) = 1 - \Phi_{prompt} - \Phi_{IC}$

$\Phi_{RISC} = \Phi_{delayed}/\Phi_{ISC}$

$k_{RISC} = (k_p k_d \Phi_{delayed})/(k_{ISC}\Phi_{prompt})$

$k_p = 1/\tau_{prompt}$; $k_d = 1/\tau_{delayed}$

Table S2. Transient PL decay data of *v*-PXZTRZ, *v*-PTZTRZ, *l*-PXZTRZ and *l*-PTZTRZ in THF/water mixtures with different water fractions (f_w).

compound	f_w	$<\tau>$ (ns)	$<\tau_1>$ (ns)	$<\tau_2>$ (ns)	A_1	A_2	R_{prompt} (%)	$R_{delayed}$ (%)
v-PXZTRZ	0	7.0	7.0	–	32267.2	–	100	0
	80	192.1	31.8	499.9	3476.9	115.2	65.8	34.2
	85	403.5	39.6	786.0	2969.5	142.3	51.3	48.7
	90	731.5	45.6	1098.8	2590.1	200.7	34.9	65.1
	95	904.9	48.3	1325.1	2529.6	188.0	32.9	67.1
	99	1177.3	47.3	1574.6	2520.5	215.4	26.0	74.0
v-PTZTRZ	0	37.9	37.9	–	3517.8	–	100	0
	80	763.0	25.6	1206.4	3873.8	136.5	37.6	62.4
	85	1601.5	28.0	2203.2	3668.6	122.0	27.6	72.4
	90	1417.1	23.8	1950.8	4139.6	131.8	27.7	72.3
	95	1478.9	25.2	2002.9	3938.3	137.2	26.5	73.5
	99	1500.6	23.6	2026.6	4183.7	137.1	26.2	73.8
l-PXZTRZ	0	9.5	2.6	10.4	1897.8	3618.9	11.6	88.4
	80	309.0	64.1	2085.83	9705.8	41.1	87.9	12.1
	85	75.5	44.0	126.9	10442.2	2218.5	62.0	38.0
	90	199.7	72.7	1808.4	8961.4	28.4	92.7	7.3
	95	465.0	78.0	2815.7	8726.1	39.8	85.9	14.1
	99	487.7	83.3	2722.8	8326.8	46.1	84.7	15.3
l-PTZTRZ	0	2.9	2.9	–	4826.9	–	100	0
	80	678.7	44.2	1829.2	10138.6	135.0	64.5	35.5
	85	1052.5	43.5	2243.7	10141.5	166.5	54.1	45.9
	90	868.0	44.7	1913.3	10093.1	185.7	55.9	44.1
	95	1145.1	43.3	2389.4	9951.0	159.7	53.0	47.0
	99	1450.9	45.1	2639.2	9984.8	202.0	45.8	54.2

Table S3. EL performances of the doped OLEDs of *v*-PXZTRZ.

		maximum values				values at 1000 cd m^{-2}						
	V_{on} (V)	η_C (cd A^{-1})	η_P (lm W^{-1})	η_{ext} (%)	L (cd m^{-2})	V (V)	η_C (cd A^{-1})	η_P (lm W^{-1})	η_{ext} (%)	CIE (x,y)	λ_{EL} (nm)	RO (%)
I	3.0	37.5	36.8	11.6	5408	4.6	19.8	13.6	6.1	(0.36, 0.56)	540	47.4
II	2.8	40.7	45.6	12.6	11385	4.0	33.8	26.5	10.5	(0.40, 0.56)	550	16.7
III	2.8	36.1	37.7	11.2	16370	3.8	33.9	28.0	10.5	(0.40, 0.56)	550	6.2

[a] Abbreviations: V_{on} = turn-on voltage at 1 cd m^{-2}; η_c = current efficiency; η_p = power efficiency; η_{ext} = external quantum efficiency; CIE = Commission Internationale de I'Eclairage coordinates; λ_{EL} = electroluminescence maximum; RO = current efficiency roll-off from maximum value to that at 1000 cd m^{-2}. Device configuration: ITO/HATCN (5 nm)/TAPC (50 nm)/TCTA (5 nm)/*x* wt% *v*-PXZTRZ: TmPyPB (20 nm)/TmPyPB (40 nm)/LiF (1 nm)/Al (*x* = 10, 20, 30 for I, II, III, respectively).

Table S4. EL performances of the doped OLEDs of *v*-PTZTRZ.

		maximum values				values at 1000 cd m^{-2}						
	V_{on} (V)	η_C (cd A^{-1})	η_P (lm W^{-1})	η_{ext} (%)	L (cd m^{-2})	V (V)	η_C (cd A^{-1})	η_P (lm W^{-1})	η_{ext} (%)	CIE (x,y)	λ_{EL} (nm)	*RO* (%)
I	3.0	25.7	27.5	9.2	1837	6.4	2.6	1.3	0.86	(0.39, 0.53)	550	90.6
II	2.8	36.0	40.4	11.9	4658	4.6	10.6	7.2	3.5	(0.42, 0.54)	556	70.6
III	2.8	28.5	28.0	9.5	7038	4.2	18.0	13.5	6.0	(0.44, 0.54)	556	36.8

[a] Abbreviations: V_{on} = turn-on voltage at 1 cd m^{-2}; η_c = current efficiency; η_p = power efficiency; η_{ext} = external quantum efficiency; CIE = Commission Internationale de I'Eclairage coordinates; λ_{EL} = electroluminescence maximum; RO = current efficiency roll-off from maximum value to that at 1000 cd m^{-2}. Device configuration: ITO/HATCN (5 nm)/TAPC (50 nm)/TCTA (5 nm)/*x* wt% *v*-PTZTRZ: TmPyPB (20 nm)/TmPyPB (40 nm)/LiF (1 nm)/Al (*x* = 10, 20, 30 for I, II, III, respectively).

Table S5. EL performances of the doped OLEDs of *l*-PXZTRZ.

		maximum values				values at 1000 cd m^{-2}						
	V_{on} (V)	η_C (cd A^{-1})	η_P (lm W^{-1})	η_{ext} (%)	L (cd m^{-2})	V (V)	η_C (cd A^{-1})	η_P (lm W^{-1})	η_{ext} (%)	CIE (x,y)	λ_{EL} (nm)	*RO* (%)
I	3.2	21.6	19.9	9.2	2150	7.2	2.0	0.87	0.85	(0.23, 0.39)	492	90.8
II	2.8	34.3	38.4	11.7	3979	5.8	4.2	2.3	1.4	(0.31, 0.51)	532	88.0
III	2.8	27.7	28.9	8.9	6886	4.6	7.2	4.9	2.3	(0.38, 0.55)	546	74.2

[a] Abbreviations: V_{on} = turn-on voltage at 1 cd m^{-2}; η_c = current efficiency; η_p = power efficiency; η_{ext} = external quantum

efficiency; CIE = Commission Internationale de I'Eclairage coordinates; λ_{EL} = electroluminescence maximum; RO = current efficiency roll-off from maximum value to that at 1000 cd m^{-2}. Device configuration: ITO/HATCN (5 nm)/TAPC (50 nm)/TCTA (5 nm)/*x* wt% *l*-PXZTRZ: TmPyPB (20 nm)/TmPyPB (40 nm)/LiF (1 nm)/Al (*x* = 10, 20, 30 for I, II, III, respectively).

Table S6. EL performances of the doped OLEDs of *l*-PTZTRZ.

		maximum values				values at 1000 cd m^{-2}						
	V_{on} (V)	η_C (cd A^{-1})	η_P (lm W^{-1})	η_{ext} (%)	L (cd m^{-2})	V (V)	η_C (cd A^{-1})	η_P (lm W^{-1})	η_{ext} (%)	CIE (x,y)	λ_{EL} (nm)	RO (%)
I	3.0	25.7	26.9	9.0	2655	6.6	1.8	0.88	0.64	(0.36, 0.49)	554	92.9
II	2.8	18.7	21.1	6.7	4817	5.2	4.0	2.4	1.4	(0.44, 0.52)	568	79.1
III	2.8	10.6	11.9	3.9	5523	4.6	5.6	3.8	2.1	(0.47, 0.51)	570	46.2

[a] Abbreviations: V_{on} = turn-on voltage at 1 cd m^{-2}; η_c = current efficiency; η_p = power efficiency; η_{ext} = external quantum efficiency; CIE = Commission Internationale de I'Eclairage coordinates; λ_{EL} = electroluminescence maximum; RO = current efficiency roll-off from maximum value to that at 1000 cd m^{-2}. Device configuration: ITO/HATCN (5 nm)/TAPC (50 nm)/TCTA (5 nm)/*x* wt% *l*-PTZTRZ: TmPyPB (20 nm)/TmPyPB (40 nm)/LiF (1 nm)/Al (*x* = 10, 20, 30 for I, II, III, respectively).

S-8 Reference

1. B. M. Bell, T. P. Clark, T. S. De Vries, Y. Lai, D. S. Laitar, T. J. Gallagher, J.-H. Jeon, K. L. Kearns, T. McIntire, S. Mukhopadhyay, H.-Y. Na, T. D. Paine and A. A. Rachford, *Dyes Pigm*., 2017, **141**, 83.
2. B. Li, Z. Li, F. Guo, J. Song, X. Jiang, Y. Wang, S. Gao, J. Wang, X. Pang, L. Zhao and Y. Zhang, *ACS Appl*. *Mater*. *Interfaces*, 2020, **12**, 14233.
3. I. S. Park, S. Y. Lee, C. Adachi and T. Yasuda, *Adv*. *Funct*. *Mater*., 2016, **26**, 1813.
4. X. Yang, Q. Yu, N. Yang, L. Xue, J. Shao, B. Li, J. Shao and X. Dong, *J*. *Mater*. *Chem*. *B*, 2019, **7**, 2454.
5. L. E. Shoer, S. W. Eaton, E. A. Margulies and M. R. Wasielewski, *J*. *Phys*. *Chem*. *B*, 2015, **119**, 7635.
6. Y. Kitamoto, T. Namikawa, T. Suzuki, Y. Miyata, H. Kita, T. Sato and S. Oi, *Org*. *Electron*., 2016, **34**, 208.
7. G. Xie, X. Li, D. Chen, Z. Wang, X. Cai, D. Chen, Y. Li, K. Liu, Y. Cao and S.-J. Su, *Adv*. *Mater*., 2016, **28**, 181.
8. Q. Zhang, H. Kuwabara, W. J. P. Potscavage, Jr., S. Huang, Y. Hatae, T. Shibata and C. Adachi, *J*. *Am*. *Chem*. *Soc*., 2014, **136**, 18070.
9. H. Uoyama, K. Goushi, K. Shizu, H. Nomura and C. Adachi, *Nature*, 2012, **492**, 234.